Density Functional Theory Used in Structure Determinations and Raman Band Assignments for Pseudoisocyanine and Its Aggregate

Chu Guo, Metin Aydin, Han-Ru Zhu, and Daniel L. Akins*

Center for Analysis of Structures and Interfaces (CASI), Department of Chemistry, The City College of The City University of New York, New York, New York 10031

Received: January 28, 2002; In Final Form: March 28, 2002

We have performed quantum chemical calculations for the optimized structure and Raman vibrational frequencies—based on density functional theory at the B3LYP level and using the 6-31G(dp) basis set—for the cyanine dye cation 1,1′-diethyl-2,2′-quinocyanine, also referred to as pseudoisocyanine (PIC). We have ascertained that the equilibrium structure of ground-state PIC has near C_2 symmetry, with a 46° twist between the planes of the two quinoline moieties that are positioned about the central methine carbon. Vibrational mode analysis of the calculated Raman spectrum suggests that many of the experimentally observed Raman bands between 500 and 1800 cm^{-1} for monomeric PIC are associated with totally symmetric in-plane deformations of phenyl and/or pyridyl rings, while several weak bands below 500 cm^{-1} are attributed to out-of-plane doming and ruffling of quinoline macrocycles. We further have noted that (1) upon comparison of the Raman spectrum of PIC monomer with the Raman spectrum measured for aggregated PIC, under nonresonant condition, changes reveal that aggregation results in enhanced scattering for specific vibrational modes that contain principal contributions from in-plane deformation of the phenyl ring in the quinoline moiety; (2) with resonant excitation for the aggregate, observed vibrational modes associated with out-of-plane distortions of the quinoline macrocycle are found to exhibit even greater enhancement. Analysis of our Raman measurements for monomeric and aggregated PIC provides details about the structure of the molecular aggregate. Additionally, calculation of charge distribution, utilizing the Mulliken population analysis approach, indicates that positive and negative charges are alternately and symmetrically distributed over a conjugated ring system, and the positive charges among the peripheral hydrogens and those in the *N*-ethyl side chains are asymmetrically distributed.

I. Introduction

Cyanine dyes define a class of conjugated organic molecules that were initially extensively studied because of their commercial application as effective spectral sensitizers for semiconductors.[1] In the course of exploiting their spectral sensitizing property, it was early determined that these molecules often self-assembled to form noncovalent aggregates in the ground state, which, upon optical excitation, resulted in the formation of molecular excitonic states. These latter states were found to be dramatically different in their spectral and dynamical properties than those of the monomers from which they derive.

Experimental as well as theoretical analyses for molecular aggregates (as, for example, contained in Davydov's molecular exciton theory) suggested a somewhat simple picture of their structures,[2] their allowed energy states, and selection rules for absorption and emission of radiation.[3−8] With this foundation, experimental measurements and analyses of aggregated cyanine systems have provided some progress in the understanding of a variety of phenomena, including even the fundamental processes of energy transfer and charge separation in photosynthetic light-harvesting antenna systems.[9] Such successes have fueled expanded interest in the study of model molecular aggregate systems. Also, more recently, a great deal of interest in aggregates has been generated by efforts to provide a theoretical foundation for understanding optical dephasing of radiation emitted by aggregated molecular systems (see refs 10−14) and by the more practical concerns of exploiting the observed enhanced linear and nonlinear optical properties of aggregated molecules for optical communications and optical computing applications.[15]

Numerous studies have dealt with the formation of aggregated cyanine dye molecules in diverse environments, including adsorbed onto silver halide grains in emulsions,[16] noble metal colloidal particles,[17] colloidal semiconductor particles[18] and electrode surfaces;[19] formed at monolayer[20] and bilayers[21] interfaces; dispersed within organic polymer films[22] and low-temperature glasses;[23] intercalated within proteins[24] and DNA matrices;[25] and, recently, formed within siliceous mesoporous materials.[26] But despite these varied studies, much information about the arrangement of molecules within molecular aggregates is little more than guess work, without the benefit of unassailable measures of the interactions between the molecular constituents within aggregate structures. In fact, the fundamental question of the effective number of molecules that coherently participate in the emission process (i.e., the coherence length) and the dependence of this number on a range of dephasing interactions, which emanate from both static and dynamical interactions, have been broadly addressed by several research groups, with no definitive assessment to date.[8,27−29] What is needed, at the very least, for solid advancement in understanding in the whole area of molecular aggregate structure and dynamics is high-resolution insight into the intermolecular interactions between constituent molecules within the aggregate structure.

10.1021/jp025567b CCC: $22.00
Published on Web 04/25/2002

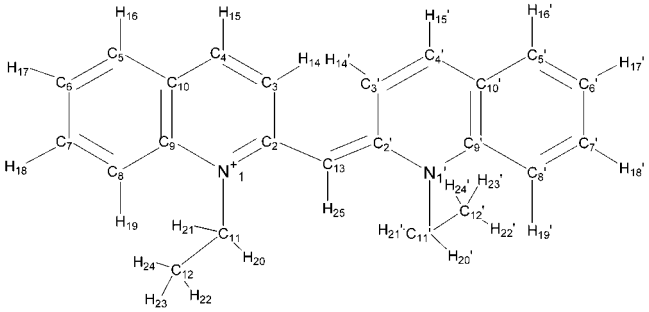

Figure 1. Molecular structure and atom numbering for PIC.

The motivation for the present investigation derives precisely from this abovementioned need. Our aim here, in broad terms, is to provide high-detailed structure information through Raman spectroscopic probing, which, in general, provides information on molecular conformations as well as on intramolecular and intermolecular interactions. Indeed, Raman scattering theoretical concepts are well developed and, in principle, allow one to decipher structure and environment information from vibrational band positions and relative intensities, provided they are attributed to appropriate normal modes of the vibrations and that these modes can be decomposed into motions of specific chromophores or bonds in the molecule. However, for essentially all of the cyanine dyes, assignments of the Raman bands have been made either on the basis of empirical comparisons of the band positions for a series of molecules with different ring constituents and spacer lengths[30−34] or through calculations based on simplified hypothetical models.[35] One finds, in general, that reported attributions of vibrational bands to specific molecular motions of the cyanine dyes have a high degree of arbitrariness and, in fact, are conflicting in many cases.

In the present paper, we report vibrational band assignments of measured Raman spectra for the prototypical cyanine dye 1,1′-diethyl-2,2′-quinocyanine, also referred to as pseudoisocyanine (PIC), see Figure 1, acquired through rigorous quantum chemical calculations based on density functional theory. Assignments of Raman bands for the PIC monomer and observed changes in vibrational band intensities upon formation of aggregated PIC, especially those bands that are enhanced upon formation of the aggregate (e.g., the J-aggregate; see ref 3), are interpreted in terms of intermolecular alignments between monomers within the aggregate. We also calculate charge distributions in the equilibrium ground configuration of the PIC monomer and use the distribution to suggest the extended structure of the molecular aggregate.

II. Computational Methods and Experimental System

Calculations. The geometry of ground-state cationic PIC was optimized with no restriction on the symmetry of the initial structure. Both structure optimization and vibrational analysis calculations were implemented by using density functional theory (DFT) with functionals,[36] specifically, B3LYP, in which the exchange functional is of the Becke's three parameter type, including gradient correction,[37]and the correlation correction involves the gradient-corrected functional of Lee, Yang and Parr.[38] The basis set of split valence type 6-31G(dp),[39] as contained in the Gaussian 98 software package, was used.[40] The vibrational mode descriptions were made on the basis of calculated nuclear displacements associated with measured vibrational frequencies, combined with visual inspection of the animated normal modes, to assess which bond and angle motions dominate the mode dynamics for the molecule.

The DFT method was chosen because it is computationally less demanding than other approaches as regards inclusion of electron correlation. Moreover, in addition to its excellent accuracy and favorable computation expense ratio,[41] the B3LYP calculation of Raman frequencies has shown its efficacy in numerous earlier studies by other researchers, often proving itself the most reliable and preferable method for many molecular species of intermediate size,[42] including anions[43] and cations.[44]

Experimental Section. The Raman spectrum of monomeric PIC (purchased from Kodak as the chloride salt, and purified further by HPLC) was acquired using methanol as the solvent. A solution of ca. 10^{-3} M was placed in a spinning cell and excited with 647 nm radiation from a Spectra-Physics 165 krypton ion laser. All samples were kept in the dark prior to spectroscopic measurements.

The Raman spectrum of aggregated PIC was acquired from aqueous samples adsorbed onto a smooth polished Ag working electrode held at a potential of −0.8 V vs SCE in an electrochemical cell, with 0.1 M KCl used as the supporting electrolyte. The cell was designed with a 45° Pyrex window in near contact with the electrode surface, to minimize aperture effects associated with absorption of scattered radiation, and has been used in several earlier investigations in this laboratory.[45] For nonresonant excitation, the sample was excited with 488 nm radiation from a Coherent Innova 200 argon ion laser, while for resonant excitation at the absorption frequency of the aggregate, 583 nm, radiation from the same ion-laser pumping a Coherent 899 Ti:sapphire tunable ring laser was used.

The excitation power at the sample, for both monomer and aggregate systems described above, was maintained at ca. 40 mW, and the Raman signals were detected with a 0.6 m Spex 1877 spectrometer that was coupled to a Spectrum-1 CCD detector cooled to 140 K with liquid nitrogen. The Raman spectra reported here have been refined by background subtraction with Microcal's Origin program. The spectral resolution for all measurements is ca. ±2 cm^{-1}. All spectroscopic measurements were conducted under ambient temperature condition.

The computer system on which quantum chemical calculations were performed was a Compaq Alpha Server DS20E, running at 667 MHz with a 1GB memory, which is a dedicated system for calculations in our laboratory.

III. Results

A. Molecular Geometry. The ground-state geometry of the PIC cation, as mentioned above, was optimized at the B3LYP/6-31G(dp) level. The bond lengths for the optimized equilibrium structure are provided in Table 1, but bond angles are not provided since, as expected in general, they are close to 120°. Additionally, selected dihedral angles are given in Table 2 for specifying the conformation of the molecule. Atom numbering is depicted in Figure 1.

In-depth inspection of Tables 1 and 2 indicates that the DFT calculated molecular structure has near C_2 symmetry, with an axis passing through the C−H bond of the central carbon atom that connects two planar quinoline moieties. The macrocycle planes of the two quinoline moieties are found to be twisted by a dihedral angle of ca. 46°, likely attributable to the balance between van der Waals repulsion between the two hydrogen atoms attached to the carbon atom at the 3-positions of each quinoline moiety and the stabilization provided by π-conjugation across the methane bridge between the two quinoline. The ethyl groups attached to the nitrogen atoms of each quinoline ring

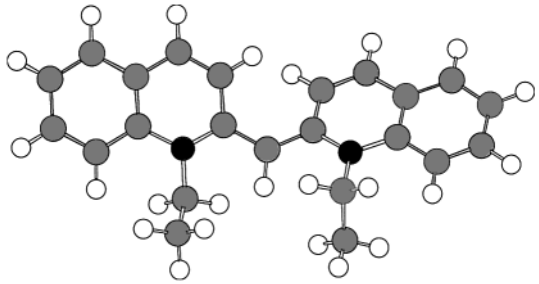

Figure 2. Optimized structure of PIC calculated using B3LYP/6-31G-(dp).

TABLE 1: Calculated PIC Bond Lengths Using B3LYP/6-31G(dp)

bond	length (Å)	bond	length (Å)
N_1-C_2	1.3814	C_3-H_{14}	1.0813
C_2-C_3	1.4334	C_4-H_{15}	1.0860
C_3-C_4	1.3597	C_5-H_{16}	1.0858
C_4-C_{10}	1.4250	C_6-H_{17}	1.0844
C_5-C_{10}	1.4109	C_7-H_{18}	1.0852
C_5-C_6	1.3809	C_8-H_{19}	1.0809
C_6-C_7	1.4042	$C_{11}-H_{20}$	1.0904
C_7-C_8	1.3872	$C_{11}-H_{21}$	1.0908
C_8-C_9	1.4100	$C_{12}-H_{22}$	1.0938
C_9-C_{10}	1.4222	$C_{12}-H_{23}$	1.0935
C_9-N_1	1.4306	$C_{12}-H_{24}$	1.0928
N_1-C_{11}	1.4818	$C_{13}-H_{25}$	1.0778
$C_{11}-C_{12}$	1.5302		
C_2-C_{13}	1.4166		

TABLE 2: Conformation of *trans*-PIC Calculated Using B3LYP/6-31G(dp)

geometry	dihedral angle	left quinoline	right quinoline
planar phenyl	$D(C_8-C_9-C_{10}-C_5)$	−1.10	−1.10
planar pyridyl	$D(C_2-C_3-C_4-C_{10})$	1.59	1.59
planar pyridyl	$D(C_2-N_1-C_9-C_{10})$	5.00	5.00
N-ethyl orientation	$D(C_3-C_2-N_1-C_{11})$	174.16	174.16
N-ethyl orientation	$D(C_{10}-C_9-N_1-C_{11})$	−172.73	−172.73
$H_{14}-C_3$ orientation	$D(C_1-C_2-C_3-H_{14})$	176.35	176.35
$H_{14}-C_3$ orientation	$D(C_{10}-C_4-C_3-H_{14})$	−174.44	−174.44
$C_{13}-H_{15}$ orientation	$D(C_3-C_2-C_{13}-H_{25})$	153.09	153.08
$C_{13}-H_{15}$ orientation	$D(N_1-C_2-C_{13}-H_{25})$	−22.91	−22.92
bridge orientation	$D(C_3-C_2-C_{13}-C_2')$	−26.91	−26.92
bridge orientation	$D(N_1-C_2-C_{13}-C_2')$	157.09	157.08

are oriented, for the ground-state equilibrium conformation, in opposite directions toward different sides of the respective macrocycle (as depicted in Figure 2; referred to as the trans conformer).

B. Atomic Charge Distribution and Dipole Moment. The atomic charge distribution calculated using B3LYP/6-31(dp) is provided in Table 3. The distribution of atomic charge has been estimated through the Mulliken population formulation as contained in Gaussian 98. This approach partitions the total charge in a molecular ion among its atoms. It is to be noted that unlike the electron charge density, atomic charge is not a quantum mechanical observable. Nevertheless, the estimation of atomic charge distribution is performed to serve as a reference for assessing the relative strengths of intermolecular interactions, as described below. Table 3 also contains the three-dimensional dipole moment based on the asymmetry in the molecular charge distribution.

The charge distribution data indicates that the charges within the PIC cation are symmetrically distributed over a conjugated system $-C_8-C_9-N_1-C_2-C_{13}-C_{2'}-N_{1'}-C_{9'}-C_{8'}-$, with alternate positive and negative charge densities for contiguous atoms, rather than localized on the amide nitrogen atom in one of the quinoline ring, as often depicted when cyanine dye molecules are drawn for visualization purposes. The heavily charge-concentrated conjugated chain is calculated as having the other carbon atoms possessing small negative charges, which, in turn, are shielded by weakly positive charged hydrogen atoms. It is also to be noted that the peripheral positively charged hydrogen atoms are asymmetrically distributed around one quinoline ring with respect to the other quinoline ring, as is also the case for the two set of ethyl hydrogens. This distortion in the symmetry of the charge distribution among the peripheral hydrogen atoms and the side chain leads to the nonzero dipole-moment components oriented in the *y*,*z*-plane (see Table 3), perpendicular to the long molecular axis passing through the two quinoline moieties.

The abovementioned calculated charge distribution is anticipated to favor an intermolecular alignment of monomers in the PIC aggregate in which they assume a spread-out card-deck geometry, which, given the twist between quinoline groups, might be expected to result in a spatially extended, intermolecular structure that is spiral in nature.

C. Spectral Assignments of Raman Bands of PIC. Vibrational analysis for the PIC cation using the B3LYP/6-31G(dp) approach produced a series of normal vibrational modes with (gas-phase) calculated frequencies and relative intensities that are fairly close to those observed experimentally for the monomer in methanol system (see Table 4).

We used the calculated frequencies in conjunction with the calculated intensity distribution to attribute observed vibrational

TABLE 3: Atomic Charge (from Mulliken Population Analysis) and Dipole Moment Using B3LYP/6-31G(dp)

atom	Mulliken charge	atom		Mulliken charge
$N^+_1(N_{1'})$	−0.611981(−0.611603)	$H_{14}(H_{14'})$		0.126600(0.135047)
$C_2(C_{2'})$	0.384533(0.382947)	$H_{15}(H_{15'})$		0.128938(0.137877)
$C_3(C_{3'})$	−0.163946(−0.164102)	$H_{16}(H_{16'})$		0.117134(0.124703)
$C_4(C_{4'})$	−0.059859(−0.059979)	$H_{17}(H_{17'})$		0.125288(0.127801)
$C_5(C_{5'})$	−0.1333381(−0.132084)	$H_{18}(H_{18'})$		0.129666(0.124622)
$C_6(C_{6'})$	−0.078188(−0.078607)	$H_{19}(H_{19'})$		0.120054(0.113967)
$C_7(C_{7'})$	−0.090050(−0.090155)	$H_{20}(H_{20'})$		0.145410(0.135166)
$C_8(C_{8'})$	−0.105739(−0.106633)	$H_{21}(H_{21'})$		0.151758 (0.138285)
$C_9(C_{9'})$	0.318517(0.318669)	$H_{22}(H_{22'})$		0.147382(0.137794)
$C_{10}(C_{10'})$	0.091901(−0.089864)	$H_{23}(H_{23'})$		0.118339(0.129340)
$C_{11}(C_{11'})$	−0.096559(−0.093225)	$H_{24}(H_{24'})$		0.134235(0.142829)
$C_{12}(C_{12'})$	−0.327595(−0.326841)	H_{25}		0.111639
C_{13}	−0.259779			
dipole moment[a] (Debye)	μ_x −0.0164	μ_y 0.7931	μ_z 0.6139	μ_{total} 1.0031

[a] The *x*-, *y*-, and *z*-directions correspond to the long axis of the molecule, the axis passing through the central methine carbon and attached hydrogen, and the axis perpendicular to the former two, respectively.

TABLE 4: Calculated and Experimental Raman Shifts of PIC

B3lyp/6-31G(dp)		experimental	
ν_{cal} (cm^{-1})	I_{rel}	ν_{exp} (cm^{-1})	I_{rel}
201.83	0.14	206	0.14
219.66	0.10	223	0.13
277.09	0.02	278	0.10
336.05	0.04	313*	0.06
379.52	<0.01	375*	0.06
428.72	0.03	423	0.04
472.12	0.05	464	0.10
503.57	0.02	491	0.12
518.97	0.04	511*	0.06
536.13	0.12	528	0.18
582.48	0.17	573	0.16
617.52	0.14	605	0.66
677.06	0.04	670	0.11
720.77	0.32	707	0.33
798.64	0.09	787	0.24
857.32	1.00	845	1.00
905.53	<0.01	890	0.19
965.07	0.05	954	0.04
1158.29	2.80	1129	0.82
1182.62	0.14	1173	0.49
1259.16	5.53	1224	1.59
1270.24	0.99	1239	1.21
1382.23	17.21	1351	1.83
1391.83	1.42	1366	1.53
1415.78	14.17	1387	2.08
1479.00	2.17	1474	0.16
1561.39	0.18	1518	0.28
1614.95	1.32	1609	0.41
1662.66	0.59	1629	0.66

[a] Intensities relative to the band at ca. 857 cm^{-1}, i.e., I_{rel}, are shown. Bands of very low intensity are labeled by *.

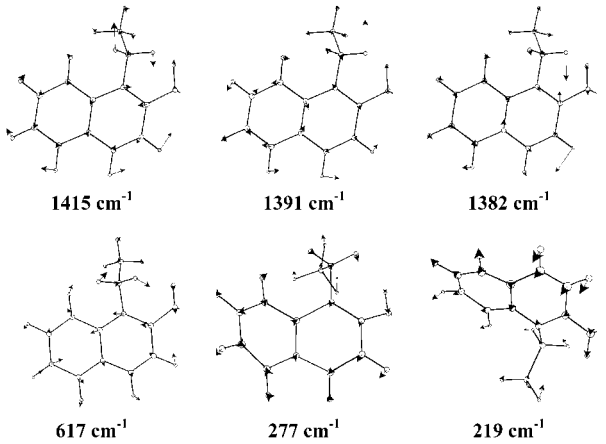

Figure 3. Normal mode displacements (enhanced by a factor of ca. 3.2) for PIC, as determined using B3LYP/6-31G(dp) theory. Only the motion of one quinoline group is shown since the other half the molecule performs an identical motion.

frequencies and intensities to specific intramolecular motions of PIC. These latter assessments were facilitated by analysis of the theoretical nuclear displacements (some examples shown in Figure 3) coupled with animation of their vibrations, to identify specific motions as the dominant movements within the molecule; this is not a truly rigorous approach but should provide correct insight. However, more rigorous potential function distribution methods will be tested in the future.

Though the animation approach, we deduced that many of the calculated molecular modes for PIC cation are composed of symmetrical motions about the methylene group bridging the two quinoline moieties. In particular, a number of the more intense Raman modes below 2000 cm^{-1} appear to be primarily associated with in-plane distortions of a quinoline macrocycle caused by stretching, in various combinations, of its skeletal bonds while at the same time the other quinoline group executes the same motion. Specific assessments of principal motions within a mode will herein be identified sequentially using Arabic numerals for ease of discussion. Thus, the calculated normal vibrational modes of frequencies 1663 and 1615 cm^{-1} (1), assigned as corresponding to the Raman features observed at 1629 and 1609 cm^{-1}, respectively, are attributed (using the visualization approach) primarily to the combination of the symmetric half-ring distortion of the phenyl group (defined by in-phase stretching of the C_5-C_6, C_8-C_9, C_6-C_7 and C_9-C_{10} bonds) concomitant with identical resolved-bond motions on the other side of the methane carbon atom. (2) The calculated vibrational mode at 1392 cm^{-1}, assigned as corresponding to the intense Raman feature observed at 1366 cm^{-1}, has as principal motions the synchronous stretching of the C_5-C_6, C_7-C_8 and C_9-C_{10} bonds of the phenyl group combined with wagging of the $C_{11}-H$ in the ethyl side chain. (3) Distortions associated with stretching of the C_9-N_1 and N_1-C_2 bonds in the pyridyl group combined with rocking of the CH_2 group in the side chain are the principal contributors to the vibrational mode at 1416 cm^{-1}, which correlates to the Raman feature at 1387 cm^{-1}. (4) The stretchings of the N_1-C_2 and C_9-C_{10} bonds and C_3-H wagging, for the 1382 cm^{-1} vibrational mode, are the principal motions for the Raman feature observed at 1351 cm^{-1}.

For observed Raman bands of moderate to low intensities, we have ascertained that the principal motions for the vibrational modes result from simultaneous, but counter distortions of the phenyl and pyridyl moieties, accompanied by related C−H band waggings. As examples, (5) the asymmetric distortion of pyridyl group coupled with asymmetric deformation of the phenyl moiety is found to be the main contributors to the vibrational mode of frequency 1270 cm^{-1}, while (6) the same asymmetric distortion of pyridyl group when coupled with the symmetrical deformation of phenyl moiety is connected with the vibrational mode at 1259 cm^{-1}. These two vibrational modes are likely associated with the observed Raman "doublet" at 1239 and 1224 cm^{-1}, respectively. Also, (7) the observed Raman band at 605 cm^{-1}, attributed to the vibrational mode at 618 cm^{-1}, is assessed as principally resulting from the symmetric distortion of the coupled phenylpyridyl moieties that leads to diagonal extension of the entire quinoline macrocycle along the axis defined by a line through the C_2 and C_6 atoms.

Additionally, we have attributed several vibrational modes for the monomer as principally resulting from out-of-plane deformations of the quinoline macrocycle. Among such modes are two with frequencies of 277 and 220 cm^{-1}, associated, respectively, with the doming and twisting of the quinoline macrocycle; or, more specifically, bending of the phenyl ring with respect to the pyridyl ring is found to make a substantial contribution to the 277-cm^{-1} band, while the major, added contribution for the 220-cm^{-1} band is mutual twisting of phenyl and pyridyl rings. The 277- and 220-cm^{-1} modes correlate, respectively, with the observed bands at 278 and 223 cm^{-1}, respectively.

It is to be noted that motions of peripheral C−H bonds, though not explicitly mentioned earlier, contribute to all of the vibrational modes described above. We have determined, in fact, that the stretchings of different C−H bonds, as expected, are the sole contributor to high-frequency Raman modes above 3000 cm^{-1}. Table 5 indicates the assignments of observed Raman features to various molecular vibrations.

TABLE 5: Local Coordinate Contributions to Calculated Raman Modes of PIC Based on B3LYP/6-31G(dp)

ν_{calc} (cm^{-1})	ν_{exp} (cm^{-1})	assignments[a]
1662.7	1629	δ(phenyl half-ring) due to $\nu(C_5-C_6)$ and $\nu(C_8-C_9)$, accompanied by weak $\nu(C_2-C_3)_{asym}$ and $\nu(C_3-C4_3)_{asym}$
1615	1609	δ(phenyl half-ring) due to $\nu(C_6-C_7)$ and $\nu(C_9-C_{10})$, accompanied by weak $\nu(C_9-N_1)_{asym}$, $\nu(N_1-C_2)_{asym}$ and CH_2 scissoring in the side chain
1561.4	1518	δ(quinoline ring)$_{asym}$ due to $\nu(C_2-C_3)_{asym}$, $\nu(C_4-C_{10})_{asym}$, $\nu(C_{10}-C_5)_{asym}$ and $\nu(C_6-C_7)_{asym}$, accompanied by C−H rocking (except for C_7−H) and CH_2 scissoring in the side chain
1479	1474	δ(quinoline ring)$_{asym}$ due to $\nu(C_{10}-C_5)_{asym}$, $\nu(C_8-C_9)_{asym}$, $\nu(C_9-N_1)_{asym}$ and $\nu(C_3-C_4)_{asym}$, accompanied by C−H rocking and CH_2 scissoring in the side chain
1415.8	1387	δ(pyridyl half-ring)$_{asym}$ due to $\nu(C_9-N_1)_{asym}$ and $\nu(N_1-C_2)_{asym}$, accompanied by CH_2 scissoring in the side chain
1391.8	1366s	δ(phenyl half-ring)$_{asym}$ due to alternating ν(C−C); accompanied by C−H bond wagging in CH_2 of the pyridyl side chain
1382.3	1351s	ν_9(pyridyl half-ring)$_{sym}$ due to $\nu(N_1-C_2)$ and $\nu(C_9-C_{10})$, accompanied by C_3−H rocking and weak C−H bond wagging in CH_2 of the side chain
1270.2	1239	(C_3−H, C_4−H) sym rocking and δ(pyridyl half-ring)$_{asym}$ due to $\nu(C_9-N_1)_{asym}$, $\nu(C_4-C_{10})_{asym}$ and side-chain torsion
1259.2	1224	(C_6−H, C_7−H) asym rocking and δ(phenyl half-ring)$_{sym}$ due to $\nu(C_8-C_9)_{sym}$, $\nu(C_{10}-C_5)_{sym}$, accompanied by $\nu(N_1-C_9)_{sym}$, $\nu(C_{10}-C_4)_{sym}$ and side-chain torsion
1182.6	1173	(C_5−H, C_6−H) asym rocking, accompanied by weak $\nu(N_1-C_{11})$ and CH_2 torsion
1158.6	1129	$\tau(CH_2)$ and CH_3 wagging in the side chain, accompanied by slight δ(quinoline)$_{asym}$ and C−H rocking
965.1	954	$\nu(C_{11}-C_{12})$ accompanied by δ(quinoline) due to out-of plane asym twisting of phenyl and pyridyl rings
905.5	890	δ(quinoline) due to ν(phenyl breathing) and δ(pyridyl deformation), accompanied by CH_2 and CH_3 wagging
857.3	845	δ(quinoline) due to δ(phenyl)$_{sym}$ accompanied by CH wagging
798.6	787	CH_2 and CH_3 rocking and $C_2-C_{13}-C_2'$ scissoring, accompanied by slight δ(quinoline) due to asym breathing of phenyl and pyridyl rings
720.8	707	δ(quinoline) due to ν(phenyl $C_5 \leftrightarrow C_8$ deformation) and ν(phenyl $C_9 \leftrightarrow C_3$ deformation)
617.5	605	δ(quinoline)due to stretching along the $C_2 \leftrightarrow C_6$ direction, accompanied by CH_2 rocking
582.5	573	δ(quinoline) due to in-plane ν(phenyl half-ring)$_{sym}$ along $C_5 \leftrightarrow C_8$ and out-of-plane ν(pyridyl half-ring)$_{sym}$ along $N_1 \leftrightarrow C_4$
536.1	528	out-of-plane δ(quinoline) due to δ(quinoline) and ν(phenyl half-ring)$_{sym}$ along $C_7 \leftrightarrow C_{10}$ and ν(pyridyl half-ring)$_{sym}$ along $C_9 \leftrightarrow C_3$
503.6	491	out-of-plane δ(quinoline) due $C_9 \leftrightarrow C_3$ stretching
472.1	464	δ(quinoline) due to in-plane twisting of the phenyl moiety with respect to the pyridyl ring, accompanied by side-chain bending
428.7	423	δ(quinoline) due to ruffling of the phenyl moiety with respect to the pyridyl ring
277.1	278	δ(quinoline) due to doming of the phenyl moiety with respect to the pyridyl ring
219.7	223	mutual twisting of quinoline moieties

[a] ν, stretching; δ, deformation; τ, torsion.

The above determinations can be summarized as follows: (a) in-plane motions of individual phenyl or pyridyl rings are major contributors to intense Raman features above 1000 cm^{-1}; (b) out-of plane distortions of the quinoline macrocycle principally contribute to the Raman features observed below 500 cm^{-1}; and (c) various deformations of the quinoline macrocycle, due to mixed distortions of both the phenyl and pyridyl rings, give rise to Raman bands of moderate to weak intensity above 500 cm^{-1}.

IV. Discussion

A. Aggregation-Induced Enhancement of Raman Bands. There are several Raman bands of the PIC cation whose decompositions into principal motions may provide high-resolution information on the intermolecular alignments of monomers within the aggregate structure. A method to make these special bands stand out from other bands is to compare Raman spectra for PIC existing as the isolated monomer versus intercalated within the aggregate. Further insight is gained by observing changes in Raman spectra of aggregated PIC under both nonresonant and resonant excitation conditions. For nonresonant excitation, the Raman spectrum should emphasize the constricted environmental (or site) influence on vibrations, while the use of resonant excitation should identify bands whose motions have major components in the aggregate formation direction that should favor coupling between the motion of the exciton and charge oscillations associated with the vibrations. Also, resonant excitation allows for the characterization of specific bands as Albrecht-type *A* and *B* terms (as discussed in the next section).[46]

Thus Figure 4 shows Raman spectra of monomeric and aggregated PIC with excitation at nonresonant wavelengths, in parts A and B, respectively. Comparison of the spectral patterns in these cases indicates that no significant shifts in spectral positions occur for any bands. However, significant differences in relative intensities are observed for many bands. For example, part B of Figure 4 when compared to part A of the same figure clearly shows a pair of enhanced features: one is a doublet near 1630 and the other a triplet near 1360 cm^{-1}, as well as an enhanced band in the low-frequency region at 605 cm^{-1}. Upon using the assignments of Raman bands for PIC cation listed in Table 5, one notes that the Raman bands are generally associated with the in-plane vibrations involving phenyl end groups, which result in altered molecular shapes. Specifically, in this regard, the enhanced Raman bands are associated with the normal vibrational modes containing symmetrical in-plane stretching of the phenyl moiety in the quinoline macrocycle; while the enhanced low-frequency feature at 605 cm^{-1}, in addition to involving distortion of the phenyl ring as a major contributor to its vibrational mode also involves a synchronous in-plane deformation of the pyridyl moiety, which leads to a diagonal extension of the full quinoline macrocycle. Thus, it appears that vibrations involving the phenyl end groups are enhanced when the molecule is part of the aggregate, even when nonresonant excitation is used. This is to be expected since $\pi-\pi^*$ interactions between aromatic phenyl chromophores are expected to play dominant roles in holding the aggregate together. And the motions of the aromatic groups, even when in-plane, are expected to be amplified through induced electronic distribution changes in adjacent phenyl groups, leading to increased polar-

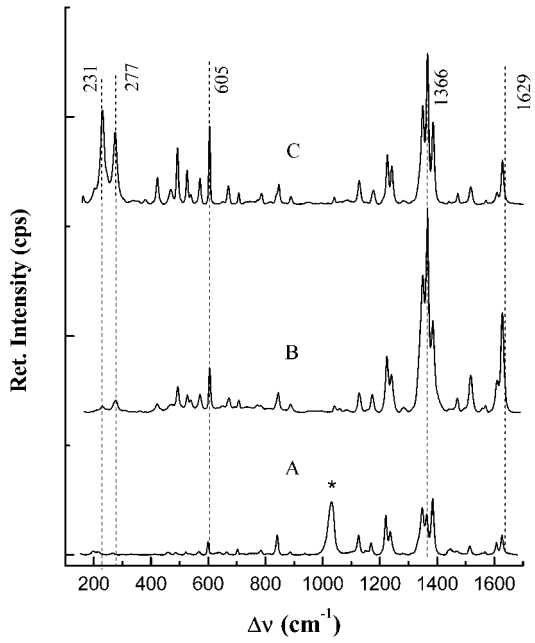

Figure 4. Raman spectra of PIC in different environments. (A) monomeric PIC in methanol; off-resonance excitation at 705 nm; 300 mW incident laser power. (B) Aggregated PIC adsorbed onto a smooth Ag-electrode held at −0.8 V vs SCE, with 0.1 M KCl as supporting electrolyte in solution; off-resonance excitation at 488 nm, 100 mW incident laser power. (C) Aggregated PIC adsorbed onto smooth Ag-electrode, with 0.1 M KCl supporting electrolyte in solution: resonance excitation at 584 nm; 20 mW incident laser radiation. The band labeled with ∗ is a solvent (i.e., methanol) band.

izability of the aggregate structure, and enhanced Raman scattering.

Of special note, in the case of the Raman spectrum of the aggregate (see Figure 4), is the pair of Raman bands at 223 and 278 cm^{-1}, which are very weak when off-resonance excitation is used but assume greatly enhanced intensity with resonance excitation (see part C of Figure 4). As mentioned earlier, the motion that dominates in both is the out-of-plane distortion of the quinoline macrocycle, to which the bending of the phenyl ring with respect to the pyridyl ring is the predominant contribution for the 277-cm^{-1} Raman band, while the major contribution for the 220-cm^{-1} band is the mutual twisting of phenyl and pyridyl rings. These determinations are consonant with the expectation that resonant excitation should identify bands whose motions have major components in the aggregate formation direction. Some more formal basis for this latter assertion is discussed in the next section, where the theoretical basis for aggregation-enhanced Raman scattering is discussed.

B. Theoretical Basis for Aggregation-Enhanced Raman Scattering (AERS). Phenomena quite similar to those described above have been addressed in several earlier papers from this laboratory that have focused on so-called aggregation-enhanced scattering (AERS) theory,[45−47] which utilizes Herzberg−Teller intensity borrowing as developed by Albrecht.[48] In these publications, one of us (D.L.A.) has shown that the enhancement of Raman bands for aggregated molecules is mainly attributable to the existence of molecular exciton states and the concomitant enhanced polarizability of the aggregate structure. The Raman intensity, which is proportional to the square of the polarizability, can be decomposed into three terms: $\alpha_{ij}^{g\upsilon',g\upsilon''} = A + B + C$, where i and j represent polarization directions, g indicates the ground electronic state, and υ' and υ'' refer to upper and lower vibrational states in the scattering problem. The C term, as has been shown earlier,[47] is expected to be less important than the A or B terms.

It has been shown that the A term explicitly involves an additivity factor N (the number of molecule participating in the coherent process), energy differences relative to the excitation frequency that lead to absorption resonances, and a factor consisting of sums over excited vibronic states of overlap integral products such as $\langle\chi_{g,\upsilon'}|\chi_{r,\upsilon}\rangle\langle\chi_{r,\upsilon}|\chi_{g,\upsilon''}\rangle$, where χ's are the vibrational wave functions and r,υ represents an excited vibronic state of the scattering species.[46] Included among the available excited vibronic states, when excitation resonant with the aggregate absorption band is used, are excited-state lattice phonon modes of the aggregate resulting from the intermolecular potential function. These latter vibrations have intercalated within them the intramolecular, single molecule vibrations and, as a result, would be expected to yield nonzero overlap integrals with appropriate intramolecular vibrations.[47,49,50] The A term is expected to dominate for certain of these bands, referred to as A-term bands, when incident radiation is close to "resonance" with the exciton absorption. In this latter case, the nonzero overlap integrals in the analytical expression for A lead to fundamental, overtone, and combination bands, usually for totally symmetric vibrational modes.[51]

But, even though the excitation conditions may correspond to a resonance situation, the B term may also be responsible for the presence of vibrational bands in the Raman spectrum. For example, for certain bands, contributions from the A term are expected to vanish. This latter situation occurs for the "strong-coupling case" for exciton formation, as detailed by Kasha,[52,53] that corresponds to little impediment for the excitation leaving the isolated single molecule and "roaming" through the aggregate structure. In such a case, the Born−Oppenheimer separability of intramolecular electronic and vibrational motions is necessitated, and since the excitation would be spread over many molecules, each individual molecule would have essentially the same electronic structure as a ground-state molecule. Thus, it would follow from the Franck−Condon principle that the A term would only be nonzero for upper state modes identical with ground-state modes. In other words, the A term would not contribute to the appearance of Raman bands resulting from the overlap of intramolecular ground and vibroexcitonic modes. On the other hand, the excited-state lattice modes of the aggregate, resulting from the intermolecular potential function, are expected to give rise to nonzero overlap integral products with ground-state intramolecular modes. Consequently, since we find for systems of aggregated molecules that the same B-term bands appear in both the resonance and nonresonance Raman spectra, we can conclude that all B-term modes are most likely fundamental, since with nonresonant excitation, these same modes, as a result of closure over excited-sate modes, must be fundamentals in the harmonic oscillator approximation.[43]

The B term, in addition to the situation discussed above, can become dominant under two other conditions. Specifically, B alone contributes to Raman bands in the nonresonant Raman case, where vibrational closure over the excited-state vibrational modes (as mentioned above) relegates the A term to make a contribution only to Rayleigh scattering; also for nontotally symmetric modes, in both the resonance and nonresonance cases, for which the A term vanishes through symmetry.

It is be noted that intensity borrowing through the Herzberg−Teller coupling term (specifically, $h_{rs}^{\alpha} \equiv \langle r|(\partial H/\partial Q_{\alpha})|s\rangle$, where H is the Hamiltonian) that appears in the analytical expression for the B term allows B to contribute to Raman scattering, and

because of its explicit dependence on the vibrational mode (α), the *B* term contributes only to intramolecular Raman modes.

It is clear that the theoretical expectations as described here are consonant with experimental finding as detailed in section IV.A above.

It is to be noted that similar Raman spectral characteristics as explained by AERS have been observed, in this laboratory, for other cyanine dyes, including 3,3′-dimethyl-9-phenyl-4,5:4′,5′-dinaphthothiacarbocyanine (NTC),[34] 1,1′-diethyl-3,3′-bis-(3-sulfopropyl)-5,5′,6,6′-tetrachlorobenzimidazolocarbocyanine (BIC, also known as TDBC-3),[54] 1,1′-3,3′-tetraethyl-5,5′,6,6′-tetrachlorobenzimidazolocarbocyanine (TTBC),[55] and 3,3′-diethyl-5,5′-dichloro-9-phenylthiacarbocyanine (DDPT).[56] Moreover, we have found a number of porphyrin derivatives that also evince aggregation-enhanced Raman scattering.[57−60]

V. Conclusion

A molecular structure calculation of PIC based on density functional theory (DFT) using the B3LYP/6-31G(dp) chemistry has yielded a molecular structure of near C_2 symmetry, with a 46° twist between the two quinoline moieties that are connected to the central methine carbon. Mulliken population analysis yields a symmetrical charge distribution that is delocalized over the ring system, with alternate positive and negative charge densities; additionally, an asymmetric distribution of the positive charge is found for peripheral hydrogen atoms and hydrogens associated with the *N*-ethyl side-chain groups.

Analyses of several of the calculated Raman modes are interpreted as indicating (a) that intense, observed bands above 1000 cm^{-1} are principally associated with totally symmetrical in-plane deformations of individual phenyl or pyridyl rings, (b) bands below 500 cm^{-1} are found to have contribution from out-of-plane distortions of the quinoline macrocycle, and (c) various in-plane deformations involving both the phenyl and pyridyl rings gives rise to Raman bands of moderate to weak intensity between 500 and ca. 1000 cm^{-1}. We further have deduced that bands that are enhanced upon formation of aggregated PIC when nonresonant excitation is used are associated with normal modes containing symmetrical in-plane stretching of the phenyl end group in the quinoline macrocycle. And we further ascertained that low-frequency bands that are enhanced upon resonance excitation of PIC aggregate, i.e., the Raman bands at 223 and 278 cm^{-1}, are associated with out-of-plane motions of the quinoline macrocycle.

Our findings regarding attribution of Raman bands to specific motions within the monomer, through the use of animation software, are supportive of the AERS formulation that has been promulgated from this laboratory. Additionally, a novel approach for deciphering the alignment of monomers within an aggregate is shown. This approach involves exploiting nonresonant radiation to assess which motions are intrinsically enhanced, simply as a result of the monomers being coupled through the dipolar forces that hold the aggregate together, and determination of which motions are in the aggregate formation direction, through acquisition of resonance Raman spectra of the aggregate. The combination of such spectra gives orientational information with vibrational resolution.

Acknowledgment. This work was supported by The National Science Foundation through the following awards: (1) IGERT program under grant DGE-9972892, (2) CIRE program under grant CHE-9872777, and (3) MRSEC program under grant DRM-9809687.

References and Notes

(1) Strumer, D. M.; Heseltine, D. W. In *The Theory of the Photographic Processes*, 4th ed.; James, T. H., Ed.; MacMillian: New York, 1977; Chapter 8.

(2) Davydov, A. S. *The Theory of Molecular Excitons*; Kasha, M., Oppenheimer, M., Jr., translators; McGraw-Hill: New York, 1962; p 174.

(3) Kasha, M.; Rawls, H. R.; El-Bayoumi, M. A. In *Molecular Spectroscopy*. Butterworth: London, 1965; p 371.

(4) Hemenger, R. P. *J. Chem. Phys*. **1976**, *66*, 1795.

(5) Kopainsky, B.; Hallermier, J. K.; Kaiser, W. *Chem. Phys. Lett.* **1982**, *87*, 7.

(6) Kemnitz, K.; Tamai, N.; Yamazaki, I.; Nakashima, N.; Yoshihara, K. *J. Phys. Chem*. **1986**, *90*, 5094.

(7) Spano, F. C.; Kuklinski, J. R.; Mukamel, S. *Phys. Rev. Lett.* **1990**, *65*, 211.

(8) Bakalis, L. D.; Knoester, J. *J. Phys. Chem. B* **1999**, *103*, 6620.

(9) *Photosynthetic Light-Harvesting Systems*; Scheer, H., Siegried, S., Eds.; W. de Gruyter: Berlin, 1988.

(10) Sundström, V.; Gillbro, T.; Gadonas, R A.; Piskarskas, A. *J. Chem. Phys*. **1988**, *89*, 2754.

(11) Van Burgel, M.; Wiersma, D. A.; Duppen, K. *J. Chem. Phys*. **1995**, *102*, 20.

(12) Kamalov, V. F.; Struganova, I. A.; Yoshihara, K. *J. Phys. Chem*. **1996**, *100*, 8640.

(13) Chakrabarti, A.; Schmidt, A.; Valencia, V.; Fluegel, B.; Mazumdar, S.; Armstrong, N.; Peyghambarian, N. *Phys. Rev. B* **1998**, *57*, R4206.

(14) Moll, J.; Harrison, W. J.; Brumbaugh, D. V.; Muenter, A. A. *J. Phys. Chem. A* **2000**, *104*, 8847.

(15) Mal'tsev, E. I.; Lypenko, D. A.; Shapiro, B. I.; Brusentseva, M. A.; Milburn, G. H. W.; Wright, J.; Hendriksen, A.; Berendyaev, V. I.; Kotov, B. V.; Vannikov, A. V. *Appl. Phys. Lett.* **1999**, *75*, 1896.

(16) Muenter, A. A.; Brumbaugh, D. V.; Apolito, J.; Hom. L. A.; Spano, F. C.; Mukamel, S. *J. Phys. Chem.* **1992**, *96*, 2783.

(17) Akins, D. L. *J. Colloid Interface Sci.* **1982**, *90*, 373.

(18) Herz, A. H. *Adv. Colloid Interface Sci*. **1977**, *18*, 375.

(19) Akins, D. L.; Macklin, J. W.; Zhu, H.-R. *J. Phys. Chem.* **1992**, *96*, 4515.

(20) Vranken, N.; Van der Auweraer, M.; De Schryver, F. C. *Langmuir* **2000**, *16*, 9518.

(21) Vranken, N.; Van der Auweraer, M.; De Schryver, F. C.; Lavoie, H.; Bélanger, P.; Salesse, C. *Langmuir* **2000,** *16*, 9518.

(22) Sluch, M. I.; Vitukhnovsky, A. G.; Yonezawa, Y.; Sato, T.; Kunisawa, T. *Opt. Mater*. **1996**, *6*, 261.

(23) Cooper, W. *Chem. Phys. Lett*. **1970**, *7*, 73.

(24) Place, I.; Perlstein, J.; Penner, T.; Whitten, D. G. *Langmuir* **2000**, *16*, 9042.

(25) Wang, M.; Silva, G. L.; Armitage, B. A. *J. Am. Chem. Soc*. **2000**, *122*, 9977.

(26) (a) Xu, W.; Guo, H.; Akins, D. L. *J. Phys. Chem. B* **2001**, *105*, 7686. (b) Xu, W.; Guo, H.; Akins, D. L. *J. Phys. Chem. B* **2001**, *105*, 1543.

(27) Kopainsky, B.; Hallermier, J. K.; Kaiser, W. *Chem. Phys. Lett.* **1981**, *83*, 498.

(28) Spano, F. C.; Mukamel, S. *J. Chem. Phys.* **1989**, *91*, 683.

(29) von Berlepsch, H.; Böttcher, C.; Ouart, A.; Burger, C.; Dähne, S.; Kirstein, S. *J. Phys. Chem. B* **2000**, *104*, 5255.

(30) Pace, J.; Pace, E. L. *Spectrochim. Acta* **1980,** *36A*, 557.

(31) Yang, J. P.; Callender, R. H. *J. Raman Spectrosc*. **1985,** *16*, 319.

(32) Sato, H.; Kawasaki, M.; Kasatani, K.; Katsumata, M. *J. Raman Spectrosc*. **1988**, *19*, 129.

(33) Iwata, K.; Weaver, W. L.; Gustafson, T. L. *J. Phys. Chem*. **1992**, *96*, 10219.

(34) Akins, D. L.; Özçelik, S.; Zhu, H.-R.; Guo, C. *J. Phys. Chem. A* **1997**, *101*, 3251.

(35) (a) Mejean, T.; Forel, M. T. *J. Raman Spectrosc*. **1977**, *6*, 117. (b) Rayer, J. C.; Forel, M. T.; Mejean, T. *J. Raman Spectrosc*. **1980**, *9*, 125.

(36) Bartolotti, L. J.; Flurchick. In *Review in Computational Chemistry*; Lipkowitz, K. B., Boyd, D. B., Eds.; VCH Publishers Inc.: New York, 1996; Vol. 7, Chapter 4.

(37) Becke, A. D. *Phys. Rev. A* **1988**, *38*, 3098.

(38) Lee, C.; Yang, W.; Parr, R. G. *Phys. Rev. B* **1993**, *37*, 785.

(39) Gordon, M. S. *Chem. Phys. Lett.* **1980**, *76*, 163.

(40) Frisch, M. J.; Trucks, G. W.; Schlegel, H. B.; Scuseria, G. E.; Robb, M. A. Cheeseman, J. R.; Zakrzewski, V. G.; Montgomery, J. A., Jr.; Stratmann, R. E.; Burant, J. C.; Dapprich, S.; Millam, M. M.; Daniels, A. D.; Kudin, K. N.; Strain, M. C.; Farkas, O.; Tomasi, J.; Barone, V.; Cossi, M.; Cammi, R.; Mennucci, B.; Pomelli, C.; Adamo, C.; Clifford, S.; Ochterski, J.; Petersson, G. A.; Ayala, P. Y.; Cui, Q.; Morokuma, K.; Malick, D. K.; Rabuck, A. D.; Raghavachari, K.; Foresman, J. B.; Cioslowski, J.; Ortiz, J. V.; Stefanov, B. B.; Liu, G.; Liashenko, A.; Piskorz, P.; Komaromi, I.; Gommperts, R.; Martin, R. L.; Fox, D. J.; Keith, T.; Al-Laham, M. A.; Peng, C. Y.; Nanayakkara, A.; Gonzalez, C.; Challacombe, M.; Gill, P. M. W.; Johnson, B. G.; Chen, W.; Wong, M. W.; Andres, J. L.; Head-Gordon,

M.; Replogle. E. S.; Pople, J. A. *Gaussian 98*, revision A.7; Gaussian, Inc.: Pittsburgh, PA, 1998.
(41) Scott, A. P.; Radom, L. *J. Phys. Chem*. **1996**, *100*, 16502.
(42) El-Azhary, A. A.; Suter, H. U. *J. Phys. Chem.* **1996**, *100*, 15056.
(43) (a) King, R. A.; Mastryukov, V. S.; Schaefer, H. F., III. *J. Chem. Phys*. **1996**, *105*, 6880. (b) King, R. A.; Galbraith, J. M.; Schaefer, H. F., III. *J. Phys. Chem*. **1996**, *100*, 6061. (c) van Huis, T. J.; Galbraith, J. M.; Schaefer, H. F., III. *Mol. Phys*. **1996**, *89*, 607. (d) Tschumper, G. S.; Fermann, J. T.; Schaefer, H. F., III. *J. Chem. Phys*. **1996**, *104*, 3676. (e) El-Azhary, A. A.; Suter, H. U.; Kubelka, J. *J. Phys. Chem*. *A* **1998**, *102*, 620. (f) Andruniow, T.; Pawlikowski, M. *Acta Phys. Pol*. **1998**, *93*, 707.
(44) (a) Brouwer, A. M. *J. Phys. Chem. A* **1997**, *101*, 3626. (b) Pan, D.-H.; Phillips, D. L. *J. Phys. Chem*. *A* **1999**, *103*, 4737. (c) Pan, D.-H.; Shoute, L. C. T.; Phillips, D. L. *J. Phys. Chem*. *A* **1999**, *103*, 6851. (d) Balakrishnan, G.; Offersgard, J. F.; Wilbrndt. *J. Phys. Chem. A* **1999**, *103*, 10798.
(45) Akins, D. L.; Zhuang, Y. H.; Zhu, H.-R.; Liu, J. Q. *J. Phys. Chem.* **1994**, *98*, 1068.
(46) Akins, D. L. *J. Phys. Chem.* **1986**, *90*, 1530.
(47) D. L. Akins, C. Akpabli and X. Li, *J. Phys. Chem.* **1989**, *93*, 1977.
(48) Albrecht, A. C. *J. Chem. Phys.* **1961**, *34*, 1476.
(49) Akins, D. L.; Lombardi, J. R. *Chem. Phys. Lett.* **1987**, *136*, 495.
(50) Akins, D. L.; Macklin, J. W.; Parker, L. A.; Zhu, H.-R. *Chem. Phys, Lett.* **1990**, *169*, 564.
(51) Akins, D. L.; Macklin, J. W. *J. Phys. Chem.* **1989**, *93*, 5999.
(52) Kasha, M. *Radiat. Res*. **1963**, *20*, 55.
(53) McRae, E. G.; Kasha, M. *Physical Processes in Radiation Biology*; Academic Press: New York, 1963; p 23.
(54) Özçelik, S.; Özçelik, I.; Akins, D. L. *Appl. Phys. Lett.* **1998**, *73*, 1949.
(55) Özçelik, S.; Akins, D. L. *Appl. Phys. Lett.* **1997**, *71*, 3057.
(56) Özçelik, S.; Akins, D. L. *J. Phys. Chem. B* **1999**, *103*, 8926.
(57) Akins, D. L.; Zhu, H.-R.; Guo, C. *J. Phys. Chem.* **1994**, *98*, 3612.
(58) Akins, D. L.; Zhu, H.-R.; Guo, C. *J. Phys. Chem.* **1996**, *100*, 5420.
(59) Akins, D. L.; Özçelik, S.; Zhu, H.-R.; Guo, C. *J. Phys. Chem.* **1996**, *100*, 14390.
(60) Guo, C.; Ren, B.; Akins, D. L. *J. Phys. Chem. B* **1998**, *102*, 8751.